nature chemical biology

ARTICLE

PUBLISHED ONLINE: 2 FEBRUARY 2015 | DOI: 10.1038/NCHEMBIO.1750

Lipid vesicles trigger α-synuclein aggregation by stimulating primary nucleation

Céline Galvagnion, Alexander K Buell, Georg Meisl, Thomas C T Michaels, Michele Vendruscolo, Tuomas P J Knowles & Christopher M Dobson*

α-Synuclein (α-syn) is a 140-residue intrinsically disordered protein that is involved in neuronal and synaptic vesicle plasticity, but its aggregation to form amyloid fibrils is the hallmark of Parkinson's disease (PD). The interaction between α-syn and lipid surfaces is believed to be a key feature for mediation of its normal function, but under other circumstances it is able to modulate amyloid fibril formation. Using a combination of experimental and theoretical approaches, we identify the mechanism through which facile aggregation of α-syn is induced under conditions where it binds a lipid bilayer, and we show that the rate of primary nucleation can be enhanced by three orders of magnitude or more under such conditions. These results reveal the key role that membrane interactions can have in triggering conversion of α-syn from its soluble state to the aggregated state that is associated with neurodegeneration and to its associated disease states.

Substantial evidence links α-syn, a small (14 kDa) highly conserved presynaptic protein, to both familial and sporadic types of PD[1–7]. When isolated in solution, α-syn is intrinsically disordered, but in the presence of lipid surfaces the protein adopts a highly helical structure[8–14] that is believed to mediate its normal functions, including control of synaptic membrane processes and biogenesis, regulation of neurotransmitter release and synaptic plasticity and modulation of neuronal survival[2,6,15–19]. The interaction between α-syn and lipids has also been shown to modulate amyloid fibril formation in different ways depending on the relative proportion of the two species[20–25]. Recent studies have suggested that α-syn may coaggregate with lipid molecules upon amyloid formation and that the lipid/protein ratio can affect the morphology of the amyloid fibrils[26], indicating the importance of achieving a global understanding of the effect of lipids on the kinetics of amyloid formation by α-syn.

In this study, we identify by means of a combination of experimental and theoretical approaches a mechanism through which small unilamellar vesicles (SUVs) prepared from the phospholipid 1,2-dimyristoyl-*sn*-glycero-3-phospho-L-serine (DMPS) perturb the kinetics of α-syn amyloid formation[27–29]. Our findings indicate that the presence of SUVs can enhance the rate of the essential primary nucleation step that initiates amyloid formation by three orders of magnitude or more, providing a global explanation of the marked modulation of the kinetics of α-syn amyloid formation by lipid vesicles[20,22,24,25]. By contrast, under these conditions other microscopic processes, including homogeneous primary nucleation in bulk solution, secondary nucleation and fragmentation, do not contribute measurably to the aggregation reaction. These results provide a mechanistic description of the key role that specific membrane interactions can have in triggering conversion of α-syn from its soluble state into the aggregated state that is associated with neurodegenerative disease.

RESULTS

The kinetics of α-syn aggregation are modulated by SUVs

In this study, we chose to work with a physiologically relevant lipid, phosphatidylserine, which, together with phosphatidylcholine and phosphatidylethanolamine, is one of the most abundant components of the membranes of synaptic vesicles[30]. To probe the influence of lipid vesicles on the aggregation behavior of α-syn, we first investigated the interaction between the protein and SUVs prepared from DMPS using CD spectroscopy (**Fig. 1a** and **Supplementary Results**, **Supplementary Fig. 1a**). We monitored the change in the mean residue ellipticity of α-syn (25 μM and 50 μM) for increasing DMPS/α-syn ratios, and the data are consistent with a single-step mode of binding (**Fig. 1a**) with a dissociation constant, K_D, of $3.8 \pm 1.3 \times 10^{-7}$ M (mean ± s.d.) and a stoichiometry, L, of 28.2 ± 0.8, where L is the total number of DMPS molecules in the bilayer that are involved in binding one molecule of α-syn. Notably, the size of the vesicles in the range of 20 nm to 100 nm does not detectably affect the affinity of the protein for the vesicles (**Supplementary Fig. 1b**). It is also interesting to note that if we assume that the lipid-bound protein molecules occupy a shell of 5-nm thickness on the external surfaces of the SUVs, by taking the hydrodynamic radius of the protein to be 26 Å (ref. 31) we can convert this stoichiometry into a local effective concentration of ~36 mM (Online Methods), which is nearly 10^3 times higher than that in bulk solution. We then monitored the kinetics of aggregation of α-syn in the presence of these SUVs at 30 °C under quiescent conditions using different DMPS/α-syn ratios (**Fig. 1b–d**).

In the absence of SUVs under these conditions, no increase in the fluorescence signal of thioflavin T (ThT) was observed over more than 65 h, indicating the absence of detectable amyloid formation[22]. Similarly, no increases in ThT fluorescence were detected when α-syn (50 μM) was incubated in the presence of an excess of DMPS SUVs (DMPS/α-syn > 40), i.e., when the protein mainly populates the lipid-bound monomeric α-helical state (**Fig. 1a**); this finding is consistent with, and indeed rationalizes, previous conclusions that the presence of lipid vesicles can inhibit amyloid formation by α-syn[24,25,32]. In addition, however, when short preformed fibrils (20 μM) were incubated with an excess of DMPS SUVs (2 mM, 4 mM and 8 mM; DMPS/α-syn > 100), the protein was found to dissociate from the fibrils (**Fig. 2a**) and to populate the lipid-bound monomeric α-helical state (**Fig. 2b**; Online Methods). This transition most likely occurs via the dissociation from the fibrils of monomeric α-syn, which, once free in solution, can bind the SUVs; indeed, the slow timescale of the equilibration, ~3 h (**Fig. 2a**), is consistent with this mechanism (Online Methods). This observation, together with the K_D value measured for the interaction between α-syn and SUVs, indicates that the lipid-bound α-helical

Department of Chemistry, University of Cambridge, Cambridge, UK. *e-mail: cmd44@cam.ac.uk

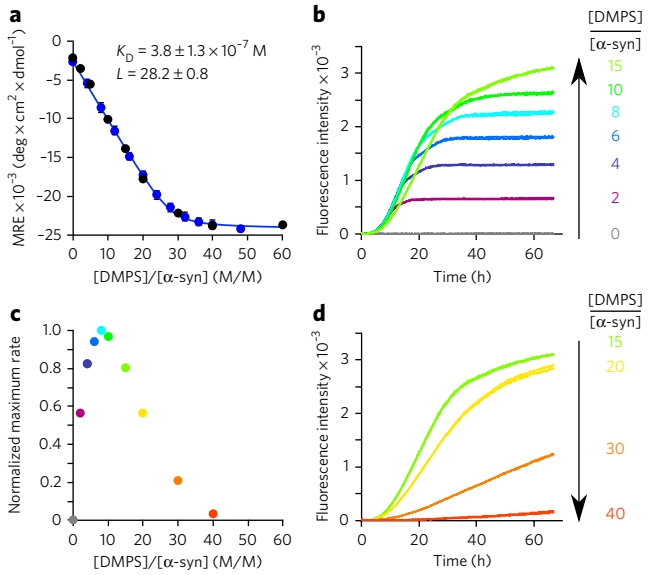

Figure 1 | Modulation of the kinetics of α-synuclein amyloid formation by lipid vesicles. (**a**) Change in the CD signal of α-syn (blue, 25 μM; black, 50 μM) measured at 222 nm as a function of [DMPS]/[α-syn] (M/M) ratios. The data (blue dots, 25 μM) fit well to a single-step binding model (equation (6) in Online Methods; the fit is represented by the blue line; K_D = 3.8 ± 1.3 × 10^{-7} M and L = 28.2 ± 0.8). (**b**,**d**) Duplicates of fluorescence measurements monitored as a function of time when α-syn (50 μM) was incubated in the absence (gray) and presence of increasing concentrations of DMPS: 100 μM (purple), 200 μM (dark blue), 300 μM (blue), 400 μM (cyan), 500 μM (green), 750 μM (light green), 1,000 μM (yellow), 1,500 μM (orange), 2,000 μM (red). (**c**) Variation in the maximum rate of aggregation of α-syn with changes in the DMPS/α-syn ratio. For DMPS/α-syn ratios above 40, no stimulation of amyloid formation is observed because effectively all of the α-syn monomers required for the growth of the aggregates are bound to the surfaces of the vesicles. The data correspond to mean ± s.d.

state of α-syn is thermodynamically more stable than the fibrillar state under these conditions. Therefore, the absence of amyloid formation in the presence of high concentrations of SUVs, as well as the dissolution of preformed fibrils, can easily be rationalized as two manifestations of the high thermodynamic stability of the lipid-bound state.

By contrast, when α-syn (50 μM) was incubated at lower concentrations of DMPS (DMPS/α-syn ratios between 2 and 15), i.e., when the protein populates both the states free in solution and bound to the vesicles, rapid formation of amyloid fibrils was observed independently of the average size of the vesicles (**Supplementary Fig. 2**), the quantities of which increased steadily as the concentration of DMPS was increased (**Fig. 1b**). In addition, as the DMPS/α-syn ratio was increased, the rate of amyloid formation decreased (**Fig. 1b–d**), a finding that can be attributed to the depletion of free monomeric α-syn in solution by the presence of DMPS SUVs; a similar phenomenon has been observed for the Aβ-peptide, whose aggregation is associated with Alzheimer's disease, in the presence of polymeric nanoparticles[33]. This observed decrease of the rate of amyloid formation for high DMPS/α-syn ratios is also likely to be attributable in part to an increasing average distance between the molecules of α-syn bound to the SUVs, thus reducing its local concentration. Taken together, these results show that the maximum rate of amyloid formation by α-syn in the presence of DMPS SUVs is observed for DMPS/α-syn ratios of 8; below this value, the rate of amyloid formation is limited by the concentration of bound α-syn, whereas above this value the rate of aggregation is limited by the concentration of free monomeric protein.

We compared the binding of α-syn to DMPS SUVs in the absence and presence of added salt (25 mM and 50 mM NaCl). The affinity of α-syn for the DMPS SUVs was observed to decrease as the concentration of NaCl increased (**Fig. 3a**), as illustrated by the increase in both the stoichiometry (from ~28 (no NaCl) to ~60 (50 mM NaCl)) and the dissociation constant (from 0.38 (no NaCl) to 11 μM (50 mM NaCl)) upon addition of NaCl; this observation can be attributed to the screening of the electrostatic interactions between the negatively charged lipid polar heads of the lipid molecules and the positively charged N-terminal region of α-syn. We then monitored the formation of amyloid fibrils in the absence and the presence of 25 mM and of 50 mM NaCl (**Fig. 3b**) and observed that the kinetics of amyloid formation slowed down as the concentration of NaCl increased, suggesting that the interaction between α-syn and the DMPS SUVs is necessary to stimulate α-syn aggregation. Overall, these results reveal that the presence of SUVs very strongly enhances the rate of amyloid formation by α-syn under the conditions used here where the DMPS/α-syn ratio is lower than 40 (**Fig. 1c**), i.e., when there is free as well as bound α-syn present in solution, as we discuss further below.

α-Syn and SUVs have distinct roles in amyloid formation

The experimental data show, therefore, that there is a dynamical equilibrium between the protein free in solution and bound to vesicles. To understand the contribution of these two populations (free and bound α-syn) to the kinetics of amyloid formation, we monitored the formation of amyloid fibrils under conditions where the concentrations of α-syn free in solution (**Fig. 4a**) and bound to the vesicles (**Fig. 4b**) were systematically varied in turn by changing the total concentrations of both protein and DMPS SUVs (equations (6)–(8) in Online Methods). The concentration of protein molecules converted into fibrils, as determined by absorbance analysis (equations (9) and (10) in Online Methods), was found to be constant at ~15 μM when the concentration of DMPS was 300 μM and for all of the different initial concentrations of α-syn free in solution tested (**Fig. 4c**); it was, however, found to be proportional to the initial concentration of α-syn bound to the vesicles, with a proportionality constant of approximately 2 (**Fig. 4d**). Notably, if secondary processes such as fibril fragmentation or autocatalytic nucleation[27] were to contribute to the formation of new fibrils, the total concentration of protein converted into fibrils would be expected to approach the initial concentration of free monomeric protein (**Fig. 4c**,**d**). Our results reveal, however, that under the conditions used here, the concentration of protein converted into fibrils when

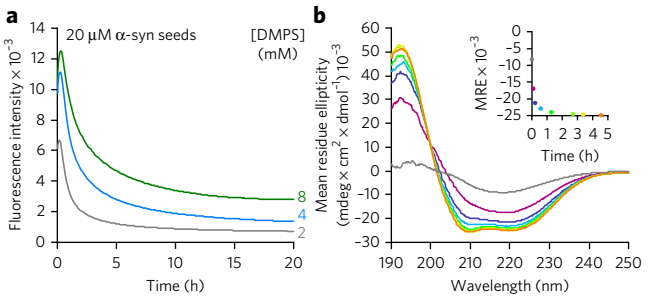

Figure 2 | Dissolution of α-syn fibrils in the presence of an excess of DMPS SUVs. (**a**) Change in the ThT fluorescence with time when 20 μM preformed amyloid fibrils were incubated in the presence of an excess of DMPS SUVs at 37 °C (gray, 2 mM; blue, 4 mM; green, 8 mM). (**b**) Change in the CD signal of α-syn when 20 μM preformed amyloid fibrils were incubated in the presence of 2 mM DMPS SUVs at 37 °C (gray, t = 0 min; purple, t = 5 min; dark blue, t = 17 min; blue, t = 39 min; green, t = 81 min; light green, t = 165 min; yellow, t = 205 min; orange, t = 275 min). Inset, change in the CD signal of α-syn measured at 222 nm as a function of time.

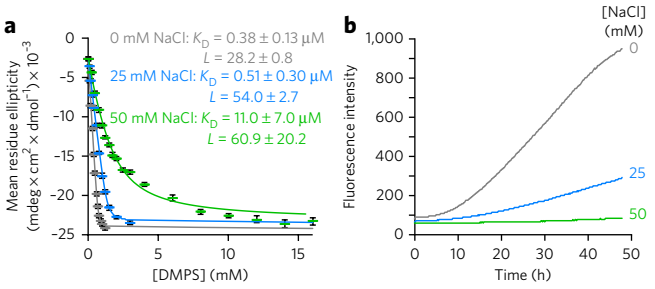

Figure 3 | Effect of the presence of salts on the binding of α-syn to DMPS SUVs and on its kinetics of amyloid formation. (**a**) Change in the CD signal measured at 222 nm of 50 μM of α-syn monitored in the presence of increasing concentrations of DMPS SUVs in the absence (gray) and the presence of 25 mM (blue) and 50 mM NaCl (green) at 30 °C. (**b**) Change in the ThT fluorescence when 50 μM α-syn is incubated in the presence of 100 μM DMPS in the absence (gray) and presence of 25 (blue) and 50 mM NaCl (green) at 30 °C. Error bars, s.d.

the aggregation kinetics had reached the plateau phase (**Fig. 4a**,**b**) did not depend on the initial concentration of free α-syn but rather on that of DMPS (**Fig. 4c**,**d**).

To probe whether the nucleation and growth of amyloid fibrils on the lipid vesicles influences the structure of the SUVs, we used membrane fluidity as observable by monitoring changes in fluorescence polarization of 1,6-diphenyl-hexa-1,3,5-triene (DPH)[34]. Markedly, the binding of monomeric α-syn to the DMPS membrane decreased its melting temperature from 41 °C to 30 °C (**Supplementary Fig. 3a**); a similar finding has been reported for DPPC membranes[35]. In addition, the fluorescence polarization of DPH when embedded within the membrane bilayers was observed to be enhanced as amyloid formation proceeded (**Supplementary Fig. 3b**), suggesting that the bilayer becomes even more rigid[34] and that the formation of amyloid fibrils does not disrupt the lipid vesicles.

Analysis using atomic force microscopy (AFM) indicated that two distinct types of structures were present in the plateau region of ThT fluorescence (**Fig. 5a**,**b**), both of which differ from those observed in the absence of SUVs (**Fig. 5c**)[36]. Some structures appear as small spherical species with a diameter of <50 nm and can be attributed to SUVs coated with α-syn molecules, and other species can be identified as thin (<5 nm in height) filaments that appear to be attached to the SUVs, and we attribute these species to amyloid fibrils whose formation had been nucleated on the surface of the SUVs. The average length of the fibrils observed by AFM is ~375 nm, a value indicating that, on average, only a single nucleation event had occurred at each vesicle (Online Methods). This observation, along with the images from the AFM analysis, shows that only a small fraction of all bound α-syn molecules contributes to the formation of an active nucleus from which a fibril can grow.

These experiments also indicate that a large proportion of monomeric protein molecules remained in solution when no further change in the ThT fluorescence intensity was observed (**Fig. 4c**), showing that amyloid formation induced by the presence of SUVs had slowed down and effectively ceased by mechanisms other than the simple depletion of free monomer generally observed during studies of amyloid formation in homogeneous solution[37]. Indeed, we isolated the remaining free monomer at the end of the first amyloid formation reaction (Online Methods) and incubated the latter with a fresh solution of DMPS SUVs (**Fig. 5d**); this incubation resulted in a second batch of fibrils with morphologies very similar to those of the species formed in the initial reaction (**Fig. 5d**). Furthermore, sonication of the reaction mixture resulted in the breakage of fibrils into small fragments (**Fig. 5e**) that, with further incubation, grew into much larger fibrils with a morphology very similar to that of fibrils formed in the absence of lipid vesicles in an agitated solution (**Fig. 5e**)[36]. These findings suggest that the end state of the aggregating solution, i.e., when the plateau in fluorescence intensity is reached, represents a kinetically trapped state due to the quiescent conditions used in these experiments. Under other conditions, the fibrils would be able to proliferate as a result of secondary processes such as fragmentation, as we show using sonication techniques. These conditions thus allow us to probe in detail the primary nucleation process that is otherwise difficult to study because, in the presence of secondary processes, the latter usually dominate the kinetics of the aggregation reaction[38].

Taken together, therefore, these observations show that the rates of secondary nucleation and fragmentation are negligible under the quiescent conditions of our experiments and that amyloid formation ceases either because of the depletion of nucleation sites on the SUVs and/or because of the inactivation of growing fibril ends, and not because of the depletion of free α-syn. These results therefore indicate that the effect of the SUVs is to enhance markedly the rate of primary nucleation of α-syn self-assembly.

Vesicles can enhance the nucleation rate by a thousandfold

Analysis of the kinetics of amyloid formation under carefully chosen and controlled conditions has been shown to enable the determination of the key microscopic steps in the mechanism of protein aggregation as well as their associated molecular rate constants[27–29,39–42]. Substantial evidence points toward the fact that heterogeneous primary nucleation, i.e., nucleation taking place at an interface such as the air-water or lipid-water interface, rather than homogeneous primary nucleation involving only free monomers in bulk solution,

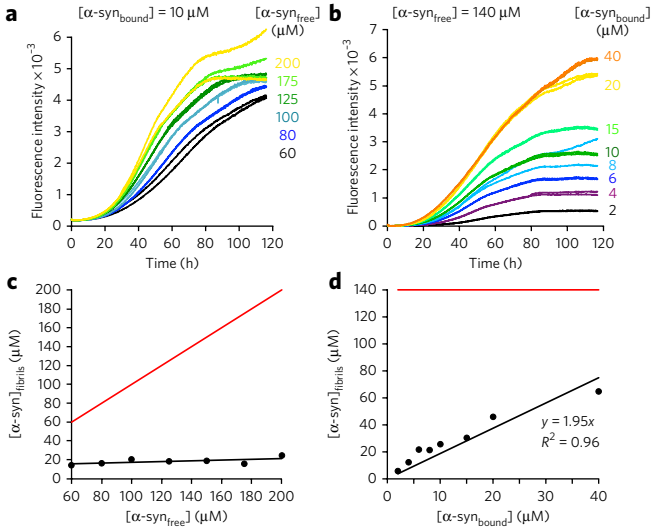

Figure 4 | Effect of the variation of the concentration of DMPS SUVs and free monomeric α-syn on the kinetics of α-syn amyloid formation. (**a**,**b**) Duplicates of the change in the fluorescence signal of ThT when increasing concentrations of α-syn (black, 60 μM; blue, 80 μM; light blue, 100 μM; dark green, 125 μM; green, 175 μM; yellow, 200 μM) were incubated in the presence of a constant concentration of DMPS (300 μM) (**a**) and when free monomeric α-syn (140 μM) was incubated in the presence of increasing concentrations of DMPS (black, 60 μM; purple, 120 μM; dark blue, 180 μM; light blue, 240 μM; dark green, 300 μM; light green, 450 μM; yellow, 600 μM; orange, 1,200 μM (**b**). (**c**,**d**) Change in the concentration of α-syn that is converted into fibrils as a function of the concentration of α-syn free in solution (**c**) or bound to the SUVs (**d**). The red lines correspond to the change in the concentration of α-syn that would be converted into fibrils as a function of the concentration of α-syn free in solution (**c**) or bound to the SUVs (**d**) if secondary processes were to dominate the kinetics of α-syn amyloid formation ([α-syn$_{fibrils}$] = [α-syn$_{total}$]$_{initial}$).

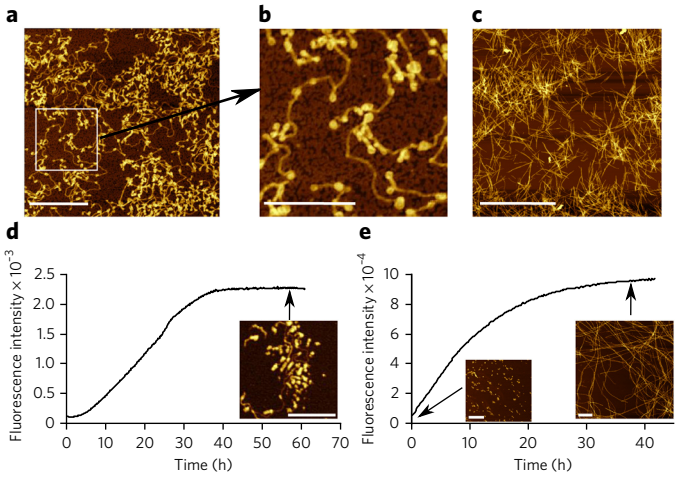

Figure 5 | Differences in the morphology of α-syn aggregates formed in the presence and absence of DMPS SUVs. (**a**,**b**) AFM images of aggregates of α-syn formed after incubation of 200 μM monomeric α-syn in the presence of 600 μM DMPS SUVs. (**b**) Expanded region of the image in **a**. (**c**) AFM image of aggregates of α-syn formed in the presence of preformed seed fibrils[36]. (**d**,**e**) Changes in the ThT fluorescence signal observed when the solution of the remaining free monomers is incubated in the presence of fresh DMPS SUVs (300 μM) (**d**) and after sonication of the reaction mixture for 10 s at the end of the process of amyloid formation (**e**). The concentrations of α-syn converted into fibrils were found to be 20 μM and 50 μM in **d** and **e**, respectively. The scale bars of the AFM images correspond to 1 μm in **a** and **e**, 500 nm in **b** and **d** and 4 μm in **c**.

is the initial step in α-syn aggregation[43–45]. We considered two possible mechanisms to describe the heterogeneous primary nucleation process accelerated by the presence of SUVs. The first and simplest is a 'one-step nucleation' model where monomers are directly converted into nuclei[46] (equations (11)–(13) in Online Methods). We also considered a more complex mechanism involving a conversion step in the nucleation process; indeed, a conversion step has been found from single-molecule experiments[47] to occur during the formation of α-syn aggregates in bulk solution under shear conditions, where initially formed disorganized oligomers were found to convert into more highly structured species. In this 'two-step nucleation' model, a prenucleus is formed and then rearranges, with a rate constant k_b, to form a growth-competent nucleus (equations (11) and (14)–(17) in Online Methods). In the analysis, we focused on the early times of the aggregation reaction, where the influence of primary nucleation is most marked. Moreover, in this regime, the concentration of monomeric protein remains constant to a good approximation, a factor that allows an analytical treatment of the rate equations[39,48]. Using this approach, we found that both models of nucleation can describe well the early time regions of the complete set of experimental curves (**Fig. 6a**,**b** and **Supplementary Fig. 4**) where our analysis is applicable (Online Methods), confirming that a greatly enhanced primary nucleation rate is the origin of the much more rapid formation of amyloid fibrils in the presence of SUVs.

Global analysis of the kinetic data, in which all of the aggregation time courses in a series of experiments are fitted with a single set of parameters, also indicates that the apparent reaction order of the nucleation step relative to free monomeric protein is ~0.2 (i.e., it is close to 0), whereas homogeneous primary nucleation rates in bulk solution typically have reaction orders greater than 1.0 (ref. 37). This observation reveals that the formation of α-syn nuclei in the presence of vesicles depends very weakly on the concentration of free monomer and therefore that free monomers are not directly involved in the rate-determining step of the nucleation process.

In addition, this analysis shows that the rate of fibril elongation from the vesicles saturates at monomer concentrations higher than ~100 μM, a value close to that observed for the saturation of the elongation of preformed fibrils in the absence of SUVs[36]. If we make the assumption that the elongation rate constant is similar in the presence of SUVs to that in their absence, the latter having been determined to be $\sim 2 \times 10^3$ M^{-1} s^{-1} (ref. 36), the rate of formation of new nuclei by α-syn at the membrane interface can be estimated from our analysis to be $\sim 1 \times 10^{-14}$ M s^{-1} at a DMPS concentration of 300 μM. This value is, remarkably, more than three orders of magnitude greater than the upper limit of the nucleation rate estimated for quiescent conditions in the absence of SUVs (7×10^{-18} M s^{-1}; Online Methods). Interestingly, an analysis using the two-step nucleation model requires a rate of conversion between the two types of nuclei of $\sim 2 \times 10^{-5}$ s^{-1}. This rate is very close to the rate of conversion between the two distinct types of oligomers observed in single-molecule experiments, 5×10^{-6} s^{-1}, in the absence of SUVs[47], suggesting that this two-step model could well apply to the type of heterogeneous nucleation in the presence of SUVs that has been identified in the present work (**Supplementary Fig. 5**).

DISCUSSION

The results described in this paper provide a self-consistent explanation for the observed modulation of α-syn amyloid formation by lipid vesicles[20,22]. At high lipid/α-syn ratios, essentially all of the protein molecules are bound to the surface of the vesicles in predominantly helical conformations[10], and, in the absence of free monomeric α-syn, aggregation does not take place at a detectable rate. At low lipid/α-syn ratios, however, when free monomer is present in solution, primary nucleation occurs on the vesicle surfaces on which α-syn is bound. The rate of this nucleation reaction is at least three orders of magnitude greater than that occurring in bulk solution, a result that can be attributed to the high local concentration of protein molecules at the surface of the vesicle and to their likely ability to explore conformations that may favor primary nucleation but are rare in solution[10]. It is important to note in this context that

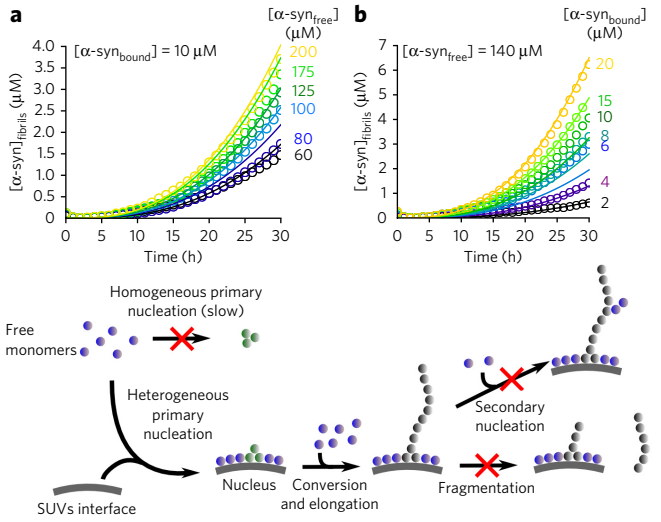

Figure 6 | Global kinetic analysis of α-syn aggregation data with a two-step nucleation model. (**a**,**b**) Global fits of the early time points of the α-syn aggregation curves obtained for the different monomer and DMPS concentrations using a two-step nucleation mechanism (equation (16) in Online Methods; $k_n k_+ = 1.2 \times 10^{-5}$ $M^{-(n+1)}$ s^{-2}, $K_M = 125$ μM, $n = 0.2$, $k_b = 1.9 \times 10^{-5}$ s^{-1}). The complete time curves are in **Figure 4a**,**b**. The scheme summarizes the proposed mechanism of amyloid formation by α-syn in the presence of DMPS SUVs on the basis of the experimental evidence described in this paper.

the magnitude by which the rate of primary nucleation is increased by lipid vesicles is likely to be affected by their composition.

Notably, it has recently been shown that the numbers of vesicles and of α-syn molecules in a functional synaptosome, or synaptic button, are ~400 and ~3,000, respectively, corresponding to an α-syn/vesicle ratio of ~10 (ref. 49). In our study, we showed that lipid vesicles enhance amyloid fibril formation when the DMPS/α-syn is below 40, corresponding to a α-syn/vesicle ratio of 100, a value one order of magnitude greater than that observed *in vivo*. Given the difference between the composition of DMPS SUVs and synaptic vesicles, however, it is noteworthy that these ratios are similar to within an order of magnitude. In addition, the fact that we have observed a closely similar enhancement of the primary nucleation rate of α-syn in the presence of both small (SUVs, <20-nm diameter) and large DMPS (large unilamellar vesicles (LUVs), >100-nm diameter) vesicles suggests that membrane curvature does not have a major role for either the binding or the nucleation of α-syn, at least under the conditions used in our study. This observation is presumably due to the fact that even the smallest vesicles do not appear curved on the scale of a protein monomer, enabling us to state that our results are relevant in the context of the vesicle sizes found *in vivo*; for example, the secretory vesicles for neurotransmitters have a diameter of ~40 nm (ref. 49).

The fact that the stimulation of amyloid formation via the enhancement of primary nucleation, the vital first step in any spontaneous aggregation process, occurs only above a threshold value of the α-syn/lipid ratio is of particular interest in the light of evidence that overexpression of α-syn via gene duplication or triplication, both of which are likely to lead to an increase in the α-syn/synaptic vesicle ratio *in vivo*, results in early onset forms of PD[19]. Such changes reflect the fact that the transition between functional interactions of α-syn with lipid membranes and deleterious ones that can generate pathogenicity is likely to be finely balanced, such that relatively small changes in concentration can cause marked increases in the risk of pathogenic behavior[50]. The present findings, therefore, contribute to our understanding of how the aggregation of α-syn *in vivo* can lead not only to a lack of functional protein molecules but also to species toxic to neuronal cells *in vivo*[2]. More generally, the discovery of the marked increase that can occur in the rate of the primary nucleation of α-syn in the presence of specific membrane surfaces provides a possible explanation of the way that the key initial steps in the process of aggregation of α-syn could occur in a cellular environment and ultimately lead to the onset and proliferation of disease.

Received 3 June 2014; accepted 17 December 2014;
published online 2 February 2015

METHODS

Methods and any associated references are available in the online version of the paper.

References

1. Bellucci, A., Navarria, L., Zaltieri, M., Missale, C. & Spano, P. α-Synuclein synaptic pathology and its implications in the development of novel therapeutic approaches to cure Parkinson's disease. *Brain Res.* **1432**, 95–113 (2012).
2. Bellucci, A. *et al.* From α-synuclein to synaptic dysfunctions: new insights into the pathophysiology of Parkinson's disease. *Brain Res.* **1476**, 183–202 (2012).
3. Chiti, F. & Dobson, C.M. Protein misfolding, functional amyloid, and human disease. *Annu. Rev. Biochem.* **75**, 333–366 (2006).
4. Dobson, C.M. Protein misfolding, evolution and disease. *Trends Biochem. Sci.* **24**, 329–332 (1999).
5. Knowles, T.P., Vendruscolo, M. & Dobson, C.M. The amyloid state and its association with protein misfolding diseases. *Nat. Rev. Mol. Cell Biol.* **15**, 384–396 (2014).
6. Spillantini, M.G. & Goedert, M. The α-synucleinopathies: Parkinson's disease, dementia with Lewy bodies, and multiple system atrophy. *Ann. NY Acad. Sci.* **920**, 16–27 (2000).
7. Spillantini, M.G. *et al.* α-Synuclein in Lewy bodies. *Nature* **388**, 839–840 (1997).
8. Bodner, C.R., Dobson, C.M. & Bax, A. Multiple tight phospholipid-binding modes of α-synuclein revealed by solution NMR spectroscopy. *J. Mol. Biol.* **390**, 775–790 (2009).
9. Davidson, W.S., Jonas, A., Clayton, D.F. & George, J.M. Stabilization of α-synuclein secondary structure upon binding to synthetic membranes. *J. Biol. Chem.* **273**, 9443–9449 (1998).
10. Fusco, G. *et al.* Direct observation of the three regions in α-synuclein that determine its membrane-bound behaviour. *Nat. Commun.* **5**, 3827 (2014).
11. Middleton, E.R. & Rhoades, E. Effects of curvature and composition on α-synuclein binding to lipid vesicles. *Biophys. J.* **99**, 2279–2288 (2010).
12. Ouberai, M.M. *et al.* α-Synuclein senses lipid packing defects and induces lateral expansion of lipids leading to membrane remodeling. *J. Biol. Chem.* **288**, 20883–20895 (2013).
13. Shvadchak, V.V., Yushchenko, D.A., Pievo, R. & Jovin, T.M. The mode of α-synuclein binding to membranes depends on lipid composition and lipid to protein ratio. *FEBS Lett.* **585**, 3513–3519 (2011).
14. Trexler, A.J. & Rhoades, E. α-Synuclein binds large unilamellar vesicles as an extended helix. *Biochemistry* **48**, 2304–2306 (2009).
15. Abeliovich, A. *et al.* Mice lacking α-synuclein display functional deficits in the nigrostriatal dopamine system. *Neuron* **25**, 239–252 (2000).
16. Clayton, D.F. & George, J.M. The synucleins: a family of proteins involved in synaptic function, plasticity, neurodegeneration and disease. *Trends Neurosci.* **21**, 249–254 (1998).
17. Fortin, D.L., Nemani, V.M., Nakamura, K. & Edwards, R.H. The behavior of α-synuclein in neurons. *Mov. Disord.* **25** (suppl. 1): S21–S26 (2010).
18. Gureviciene, I., Gurevicius, K. & Tanila, H. Role of α-synuclein in synaptic glutamate release. *Neurobiol. Dis.* **28**, 83–89 (2007).
19. Nemani, V.M. *et al.* Increased expression of α-synuclein reduces neurotransmitter release by inhibiting synaptic vesicle reclustering after endocytosis. *Neuron* **65**, 66–79 (2010).
20. Auluck, P.K., Caraveo, G. & Lindquist, S. α-Synuclein: membrane interactions and toxicity in Parkinson's disease. *Annu. Rev. Cell Dev. Biol.* **26**, 211–233 (2010).
21. Butterfield, S.M. & Lashuel, H.A. Amyloidogenic protein-membrane interactions: mechanistic insight from model systems. *Angew. Chem. Int. Edn Engl.* **49**, 5628–5654 (2010).
22. Fink, A.L. The aggregation and fibrillation of α-synuclein. *Acc. Chem. Res.* **39**, 628–634 (2006).
23. Giehm, L., Svergun, D.I., Otzen, D.E. & Vestergaard, B. Low-resolution structure of a vesicle disrupting α-synuclein oligomer that accumulates during fibrillation. *Proc. Natl. Acad. Sci. USA* **108**, 3246–3251 (2011).
24. Martinez, Z., Zhu, M., Han, S. & Fink, A.L. GM1 specifically interacts with α-synuclein and inhibits fibrillation. *Biochemistry* **46**, 1868–1877 (2007).
25. Zhu, M. & Fink, A.L. Lipid binding inhibits α-synuclein fibril formation. *J. Biol. Chem.* **278**, 16873–16877 (2003).
26. Hellstrand, E., Nowacka, A., Topgaard, D., Linse, S. & Sparr, E. Membrane lipid co-aggregation with α-synuclein fibrils. *PLoS ONE* **8**, e77235 (2013).
27. Cohen, S.I., Vendruscolo, M., Dobson, C.M. & Knowles, T.P. From macroscopic measurements to microscopic mechanisms of protein aggregation. *J. Mol. Biol.* **421**, 160–171 (2012).
28. Cohen, S.I. *et al.* Nucleated polymerization with secondary pathways. I. Time evolution of the principal moments. *J. Chem. Phys.* **135**, 065105 (2011).
29. Knowles, T.P. *et al.* An analytical solution to the kinetics of breakable filament assembly. *Science* **326**, 1533–1537 (2009).
30. Takamori, S. *et al.* Molecular anatomy of a trafficking organelle. *Cell* **127**, 831–846 (2006).
31. Dedmon, M.M., Lindorff-Larsen, K., Christodoulou, J., Vendruscolo, M. & Dobson, C.M. Mapping long-range interactions in α-synuclein using spin-label NMR and ensemble molecular dynamics simulations. *J. Am. Chem. Soc.* **127**, 476–477 (2005).
32. Zhu, M., Li, J. & Fink, A.L. The association of α-synuclein with membranes affects bilayer structure, stability, and fibril formation. *J. Biol. Chem.* **278**, 40186–40197 (2003).
33. Cabaleiro-Lago, C., Quinlan-Pluck, F., Lynch, I., Dawson, K.A. & Linse, S. Dual effect of amino modified polystyrene nanoparticles on amyloid β protein fibrillation. *ACS Chem Neurosci* **1**, 279–287 (2010).
34. Lentz, B.R. Use of fluorescent probes to monitor molecular order and motions within liposome bilayers. *Chem. Phys. Lipids* **64**, 99–116 (1993).
35. Nuscher, B. *et al.* α-Synuclein has a high affinity for packing defects in a bilayer membrane: a thermodynamics study. *J. Biol. Chem.* **279**, 21966–21975 (2004).
36. Buell, A.K. *et al.* Solution conditions determine the relative importance of nucleation and growth processes in α-synuclein aggregation. *Proc. Natl. Acad. Sci. USA* **111**, 7671–7676 (2014).
37. Cohen, S.I. *et al.* Proliferation of amyloid-β42 aggregates occurs through a secondary nucleation mechanism. *Proc. Natl. Acad. Sci. USA* **110**, 9758–9763 (2013).

38. Meisl, G. *et al.* Differences in nucleation behavior underlie the contrasting aggregation kinetics of the Aβ40 and Aβ42 peptides. *Proc. Natl. Acad. Sci. USA* **111**, 9384–9389 (2014).
39. Ferrone, F. Analysis of protein aggregation kinetics. *Methods Enzymol.* **309**, 256–274 (1999).
40. Ferrone, F.A., Hofrichter, J. & Eaton, W.A. Kinetics of sickle hemoglobin polymerization. II. A double nucleation mechanism. *J. Mol. Biol.* **183**, 611–631 (1985).
41. Oosawa, F. & Kasai, M. A theory of linear and helical aggregations of macromolecules. *J. Mol. Biol.* **4**, 10–21 (1962).
42. Xue, W.F., Homans, S.W. & Radford, S.E. Systematic analysis of nucleation-dependent polymerization reveals new insights into the mechanism of amyloid self-assembly. *Proc. Natl. Acad. Sci. USA* **105**, 8926–8931 (2008).
43. Campioni, S. *et al.* The presence of an air-water interface affects formation and elongation of α-synuclein fibrils. *J. Am. Chem. Soc.* **136**, 2866–2875 (2014).
44. Giehm, L., Lorenzen, N. & Otzen, D.E. Assays for α-synuclein aggregation. *Methods* **53**, 295–305 (2011).
45. Giehm, L. & Otzen, D.E. Strategies to increase the reproducibility of protein fibrillization in plate reader assays. *Anal. Biochem.* **400**, 270–281 (2010).
46. Oosawa, F. *Thermodynamics of the Polymerization of Protein* (Academic Press, 1975).
47. Cremades, N. *et al.* Direct observation of the interconversion of normal and toxic forms of α-synuclein. *Cell* **149**, 1048–1059 (2012).
48. Bishop, M.F. & Ferrone, F.A. Kinetics of nucleation-controlled polymerization. A perturbation treatment for use with a secondary pathway. *Biophys. J.* **46**, 631–644 (1984).
49. Wilhelm, B.G. *et al.* Composition of isolated synaptic boutons reveals the amounts of vesicle trafficking proteins. *Science* **344**, 1023–1028 (2014).
50. Ciryam, P., Tartaglia, G.G., Morimoto, R.I., Dobson, C.M. & Vendruscolo, M. Widespread aggregation and neurodegenerative diseases are associated with supersaturated proteins. *Cell Rep.* **5**, 781–790 (2013).

Acknowledgments

We wish to thank M. Ouberai for her help with the preparation of SUVs and for valuable discussions along with C. Waudby and J. Christodoulou. This work was supported by the UK Biotechnology and Biochemical Sciences Research Council (BB/H003843/1 to C.M.D. and M.V.); the Wellcome Trust (094425/Z/10/Z to C.M.D., T.P.J.K. and M.V.); the European Research Council (337969, T.P.J.K.); the Frances and Augustus Newman Foundation (T.P.J.K.); Magdalene College, Cambridge (A.K.B.); St John's College, Cambridge (T.C.T.M.); the Cambridge Home and EU Scholarship Scheme (G.M.); Elan Pharmaceuticals (C.M.D., T.P.J.K., M.V., C.G. and A.K.B.) and the Leverhulme Trust (A.K.B.).

Author contributions

C.G. performed the experiments and A.K.B. recorded the AFM images. C.G., A.K.B., T.P.J.K., M.V. and C.M.D. were involved in the design of the study. C.G., A.K.B., G.M. and C.M.D. wrote the paper, and all the authors were involved in the analysis of the data and editing of the paper.

Competing financial interests

The authors declare no competing financial interests.

Additional information

Supplementary information is available in the online version of the paper. Reprints and permissions information is available online at http://www.nature.com/reprints/index.html. Correspondence and requests for materials should be addressed to C.M.D.

ONLINE METHODS

Reagents. 1,2-Dimyristoyl-*sn*-glycero-3-phospho-L-serine (sodium salt; DMPS) was purchased from Avanti Polar Lipids, Inc. Sodium phosphate monobasic (NaH_2PO_4, BioPerformance Certified, ≥ 99.0%), sodium phosphate dibasic (Na_2HPO_4, ReagentPlus, ≥ 99.0%), sodium chloride (NaCl, BioXtra ≥ 99.5%), sodium azide (NaN_3, ReagentPlus, ≥ 99.5%), 1,6-diphenyl-hexa-1,3,5-triene (DPH, 98%), ethanol (EtOH, ≥ 99.8%) and Triton X-100 were purchased from Sigma Aldrich. Thioflavin T UltraPure Grade (ThT, ≥ 95%) was purchased from EUROGENTEC LTD.

Protein and lipid preparation. Wild-type α-syn was expressed and purified as previously described[36,51]. The lipids were dissolved in 20 mM phosphate buffer (NaH_2PO_4/Na_2HPO_4), pH 6.5, 0.01 % NaN_3 and stirred at 45 °C for 2 h. The solution was then frozen and thawed five times using dry ice and a water bath at 45 °C. The preparation of SUVs or LUVs was done using sonication (Bandelin, Sonopuls HD 2070, 3 × 5 min, 50% cycles, 10% maximum power) on ice or extrusion through membranes with a 100-nm pore diameter (Avanti Polar Lipids, Inc.) at 45 °C, respectively. After centrifugation, the sizes of the SUVs and LUVs were checked using dynamic light scattering (Zetasizer Nano ZSP, Malvern Instruments, Malvern, UK) and were shown to consist of a distribution centered at a diameter of 20 nm and 100 nm, respectively.

CD spectroscopy. *Sample preparation and data acquisition.* CD samples were prepared by incubating 50 μM α-syn in the presence of increasing concentrations of DMPS SUVs in 20 mM phosphate buffer, pH 6.5, 0.01 % NaN_3. Far-UV CD spectra were recorded on a JASCO J-810 equipped with a Peltier thermally controlled cuvette holder at 30 °C. Quartz cuvettes with path lengths of 1 mm were used, and CD spectra were obtained by averaging five individual spectra recorded between 250 nm and 200 nm with a bandwidth of 1 nm, a data pitch of 0.2 nm, a scanning speed of 50 nm/min and a response time of 1 s. Each value of the CD signal intensity reported at 222 nm corresponds to the average of five measurements, each acquired for 10 s. For each protein sample, the CD signal of the buffer used to solubilize the protein was recorded and subtracted from the CD signal of the protein.

Data analysis. The CD signal shown in this paper (CD_{obs}) can be described as follows:

$$CD_{obs} = x_B CD_B + x_F CD_F \quad (1)$$

where x_B and x_F are the fractions of α-syn bound to the membrane and free in solution, respectively, and CD_B and CD_F are the CD signals of the bound and free form of α-syn, respectively. By assuming that $x_B + x_F = 1$ and that the signals of α-syn in the presence of buffer or in the presence of SUVs under saturating conditions, correspond to CD_F and CD_B, respectively, the fraction of α-syn bound to the SUVs for each sample can be expressed as:

$$x_B = \frac{CD_{obs} - CD_F}{CD_B - CD_F} \quad (2)$$

We use the model $F + DMPS_L \rightleftharpoons B(DMPS)_L$ and the corresponding equations (equations (2) and (6)) to fit the data, where F and B represent α-syn free in solution and bound to the vesicles, respectively, and L is the number of DMPS molecules interacting with one molecule of α-syn.

$$K_D = \frac{[F][DMPS_L]}{[B(DMPS)_L]} \quad (3)$$

$$[\alpha\text{-syn}] = [F] + [B(DMPS)_L] \quad (4)$$

$$[DMPS] = L([DMPS_L] + [B(DMPS_L)]) \quad (5)$$

$$X_B = \frac{\left([\alpha-\text{syn}] + \frac{[DMPS]}{L} + K_D\right) - \sqrt{\left([\alpha-\text{syn}] + \frac{[DMPS]}{L} + K_D\right)^2 - \frac{4[DMPS][\alpha-\text{syn}]}{L}}}{2[\alpha-\text{syn}]} \quad (6)$$

Using the values of K_D (in M), as well as the stoichiometry, L, obtained from the fit, we estimated the concentration of the protein bound to the vesicles (b) and of the protein free in solution (m) and for any given DMPS/α-syn ratio:

$$b = x_B[\alpha-\text{syn}] \quad (7)$$

$$m = [\alpha-\text{syn}] - b \quad (8)$$

Estimation of the local concentration of α-syn at the surface of a SUV. We estimated the local concentration of α-syn at the surface of each SUV by assuming that all of the protein molecules bound to the lipid surface occupy a shell of 5-nm thickness at the outside of the SUVs on the basis of the hydrodynamic radius of monomeric α-syn in solution of 2.5 nm (ref. 31). This layer has a volume of 1.4×10^{-24} m^3 ($V = \frac{4}{3}\pi r_1^3 - \frac{4}{3}\pi r_2^3$, $r_1 = 15$ nm and $r_2 = 10$ nm). By assuming that the area per lipid of DMPS is of the order of 0.40 nm^2 (ref. 52), we estimated that ~3,140 lipid molecules of DMPS are exposed per SUV as

$$\left(\text{number of lipid exposed per vesicle} = \frac{\text{Surface of SUV}}{\text{Surface per lipid of DMPS}}\right),$$

and therefore there are a total number of ~6,000 lipid molecules of DMPS per SUV. For a given stoichiometry, L, the local concentration of α-syn at the surface of each SUV can be estimated by $[\alpha-\text{syn}]_{local} \sim \frac{6{,}000}{LN_A V}$, with N_A representing Avogadro's number and V measured in dm^3.

Analysis of the dissociation of preformed α-syn amyloid fibrils by high concentrations of SUVs. The combined CD and ThT experiments shown in **Figure 2** suggest that, even in the presence of 2 mM SUVs, 20 μM of preformed short (through sonication) fibrils[36] are quantitatively dissociated. We can use the ThT time traces to analyze the kinetics of dissociation and check whether or not they are consistent with the dissociation of monomers from the ends of the fibrils, which subsequently bind the SUVs. Therefore, free monomers are constantly removed, and the equilibrium is slowly shifted away from the fibrillar state. In principle, one would expect a constant rate of decrease of ThT fluorescence if a homogeneous population of fibrils dissociates, as each fibril will dissociate independently of the others. We observe, however, that the rate of dissociation decreases over time. This feature presumably stems from the fact that the fibrils are not monodispersed in length but rather display a distribution of lengths ranging from less than 50 nm to more than 200 nm in length[36]. Therefore, the short fibrils will vanish first, and the total number of dissociating fibrils will decrease with time, rationalizing the observed decrease in rate. For our analysis, we considered only the initial linear part of the data, where the concentration (by number) of fibrils is likely to correspond to the (known) initially added concentration.

The difference in absolute fluorescence intensity between the data in the presence of 2 mM, 4 mM and 8 mM SUVs as well as the small increase in fluorescence at the beginning of the experiments are likely to be due to effects of the lipids on the ThT fluorescence. If the curves are normalized such that the maximal values are set to 1.0 in each case, the initial rates of dissociation differ by less than a factor of two. We will use the mean of the three observed dissociation rates, 3.53×10^{-9} M s^{-1}, for our calculation of the molecular rate constant. The concentration by number of dissociating fibrils can be calculated from the average number of monomers per fibril (180 (ref. 36)) to be ~1.1×10^{-7} M. Therefore, we obtain a dissociation rate constant, k_{off}, of 3.2×10^{-2} s^{-1}. This value can be compared to that of the dissociation rate constant that can be calculated by assuming that at thermodynamic equilibrium, the growth and dissociation rates are equal. The monomer concentration at equilibrium has been reported to be ~1.6 μM (ref. 53). Together with an elongation rate constant of 2.2×10^3 M^{-1} s^{-1} (ref. 36), this value yields a dissociation rate constant, k_{off}, of 3.52×10^{-3} s^{-1}. The results of these two approaches give values that are consistent to within one order of magnitude, and indeed the apparent difference may be due to the approximations made during the calculations as well as to uncertainties in the reported values of the equilibrium free monomer concentration and the elongation rate constant. We conclude that the dissolution of the preformed fibrils upon the addition of excess concentrations of SUVs is consistent with a mechanism in which the SUVs bind most of the free monomeric α-syn molecules, which leads to a shift in the equilibrium distribution of species and to the slow disappearance of the fibrils. It is worth noting that, in this fibril dissolution experiment, both

the initial and final fluorescence intensities depend on the lipid concentration, which can be attributed to a direct ThT-lipid interaction.

Fluorescence polarization measurements. A stock solution of 2 mM DPH was prepared by solubilizing it in 100% EtOH overnight with stirring at room temperature. The dye was then diluted into a stock solution of DMPS SUVs, and the mixture was incubated at 45 °C for 30 min; the final EtOH content of this mixture was kept below 0.5%. After incubation, the size of the SUVs was checked using dynamic light scattering (Malvern Instruments, Malvern, UK) and consisted of a distribution centered at a diameter of 23 nm. The DMPS SUVs embedded with DPH were then incubated in the absence and the presence of α-syn or 10% Triton X-100, and the different solutions were placed in Corning 96-well plates with half-area (black/clear bottom polystyrene) nonbinding surfaces. The fluorescence polarization of DPH was then monitored using a plate reader (Polarstar Omega, BMG Labtech, Aylesbury, UK) under quiescent conditions at temperatures ranging from 10 °C to 60 °C. A 355-nm excitation filter and two matched emission filters (430 nm) were installed in the corresponding filter wheels.

Aggregation kinetics. *Sample preparation and data acquisition.* α-Syn was incubated in 20 mM sodium phosphate, pH 6.5, 0.01% NaN_3, in the presence of 50 μM of ultrapure ThT and increasing concentrations of DMPS SUVs. The change in the ThT fluorescence signal with time was monitored using a plate reader (BMG Labtech, Aylesbury, UK) under quiescent conditions at 30 °C. Corning 96-well plates with half-area (black/clear bottom polystyrene) nonbinding surfaces were used for each experiment. We also used polystyrene binding plates and obtained the same kinetics of amyloid formation by α-syn in the presence of DMPS SUVs as those measured using nonbinding plates. At the end of each aggregation experiment, the samples were ultracentrifuged at 90 k.r.p.m. for 30 min, and the concentration of the free monomer was calculated by measuring the UV spectrum of the supernatant and using the following expressions:

$$[\mathrm{ThT}] = \frac{\mathrm{Abs}_{410}}{\varepsilon_{\mathrm{ThT},410}} \tag{9}$$

$$[\alpha-\mathrm{syn}]_{\mathrm{monomer}} = \frac{\mathrm{Abs}_{275} - [\mathrm{ThT}]\varepsilon_{\mathrm{ThT},275}}{\varepsilon_{\alpha\text{-syn},275}} \tag{10}$$

where Abs_{275} and Abs_{410} are the absorbance values measured at 275 nm and 410 nm, respectively; $\varepsilon_{\mathrm{ThT},275}$, $\varepsilon_{\mathrm{ThT},410}$ and $\varepsilon_{\alpha\text{-syn},275}$ are the extinction coefficients of ThT at 275 nm and 410 nm and of α-syn at 275 nm, whose values were respectively taken as 3,200 M^{-1} cm^{-1}, 22,725 M^{-1} cm^{-1} and 5,600 M^{-1} cm^{-1} (ref. 54). The extinction coefficients of ThT at 275 nm and 410 nm were determined using a standard curve made by monitoring the absorbance spectra (250–600 nm) of ThT samples whose concentration ranged from 0 μM to 50 μM. The concentration of the fibrils was then estimated using the following relationship: $[\alpha - \mathrm{syn}]_{\mathrm{fibrils}} = [\alpha - \mathrm{syn}]_{\mathrm{initial}} - [\alpha - \mathrm{syn}]_{\mathrm{monomer}}$, where $[\alpha - \mathrm{syn}]_{\mathrm{initial}}$ is the concentration of α-syn at $t = 0$ in the well.

Kinetic data analysis. The general approach to modeling the kinetics of fibrillar aggregation, as outlined previously[28,29], derives differential equations for the number $P(t)$ and mass concentration $M(t)$ of fibrils, which can then be solved to give the time evolution of the aggregation reaction. The processes usually taken into account are primary nucleation followed by elongation through addition of monomers to the fibril ends. In some systems, secondary processes (i.e., formation of new growth-competent aggregates from existing aggregates, including fragmentation and heterogeneous nucleation on the surface of existing aggregates) are also relevant[36,37], but they were found to be negligible in the early time courses of the reactions studied in this work. In previous studies it has been shown that the elongation rate may saturate at high concentrations of monomeric α-syn[36], which we take account of by treating elongation as a Michaelis-Menten–like process[55]. The resulting differential equation for the formation of fibril mass, M(t), is given by:

$$\frac{dM}{dt} = k_+ \frac{m(t)}{1+\frac{m(t)}{k_M}} P(t) \tag{11}$$

where k_+ is the elongation rate constant, m(t) is the free monomer concentration, P(t) is the number concentration of fibrils, and K_M is the Michaelis constant, which gives the monomer concentration at which saturation effects become important[55]. We then consider two different possible nucleation mechanisms to obtain the equations for the variation in fibril numbers:

Single-step nucleation. The simplest model is a nucleated growth model[46]. As the present system involves nucleation only at the surface of vesicles (heterogeneous primary nucleation), we assume that the rate of heterogeneous primary nucleation also depends on the concentration, 'b', of bound α-syn. The corresponding differential equation is given by:

$$\frac{dP}{dt} = k_n b m(t)^n \tag{12}$$

where k_n is the heterogeneous primary nucleation rate constant and n is the reaction order of the heterogeneous primary nucleation reaction relative to the free monomer, m(t). Note that for systems with a constant concentration of bound α-syn, this process is equivalent to simple homogeneous nucleation in solution with an effective rate constant of $k_n b$. It is clear that the concentration of 'active' bound α-syn, i.e., bound α-syn that is able to form nuclei, will decrease over the course of a reaction, as free monomer remains at the plateau phase of the reaction, and therefore heterogeneous nucleation processes must have ceased to produce new growth-competent nuclei. In the present study, we focused on the early time points in the overall reaction, when this effect is unlikely to have any major role. In the early time limit, we can set $m(t) = m(0)$, which is equivalent to assuming that the depletion of monomer is insignificant for early times. Equations (11) and (12) can easily be solved and yield for the case of an unseeded reaction:

$$M(t) = \frac{K_M k_+ m(0)^{n+1} k_n b t^2}{2(K_M + m(0))} \tag{13}$$

Note the characteristic t^2 dependence that arises from this expression.

Two-step nucleation. At the next stage of complexity, we introduce one conversion step into the heterogeneous primary nucleation process: the first step of the productive nucleation process is the formation of a prenucleus, A, which then rearranges with rate constant k_b to form a growth competent nucleus. The relevant equations are:

$$\frac{dA}{dt} = k_n b m(t)^n - k_b A(t) \tag{14}$$

$$\frac{dP}{dt} = k_b A(t) \tag{15}$$

As before, the solutions for the early time limit can easily be derived, yielding:

$$M(t) = \frac{K_M k_n m(0)^{n+1} b}{k_b^2 (K_M + m(0))} \left(-k_+ (e^{-k_b t} - 1) + \frac{k_+ k_b^2 t^2}{2} - k_b k_+ t \right) \tag{16}$$

Expansion of the exponential for the short time gives a t^3 leading term (equation (17)), predicting a sharper increase in aggregate concentration in the two-step nucleation mechanism than that predicted in the single-step nucleation mechanism.

$$M(t) = \frac{K_M k_n m(0)^{n+1} b k_b k_+ t^3}{6(K_M + m(0))} \tag{17}$$

We note that in the regime where we observe stimulation of α-syn aggregation by SUVs, the local concentration of the protein at the surface of the vesicles is essentially constant. In fact, a change in lipid concentration leads only to a change in the total macroscopic concentration of bound protein and not to a change in the local concentration of the protein at the surface of each vesicle. Therefore, the reaction order of the nucleation step with respect to bound protein is not accessible through our current experimental strategy. An increase in lipid concentration will indeed lead to a proportional increase in nucleation rate simply owing to the fact that there is a larger lipid surface for the nucleation to take place on.

Fitting of the kinetic data. The above early time solutions (equations (13) and (16)) were used to fit globally the first 30 h of the kinetic traces at all the monomer and lipid concentrations shown in **Figure 6** and **Supplementary Figure 4**. The fits were performed using the Knowles group online aggregation

doi:10.1038/nchembio.1750

fitter (http://www.amylofit.ch.cam.ac.uk/), which is based on a basin-hopping algorithm[56]. The residuals are the difference between the fitted curves and the experimental values (average this over the repeats) at each data point (**Supplementary Fig. 5**). The mean squared error of the fits (as indicated in the legends of **Supplementary Fig. 5**) is the sum of all squared residuals over the number of data points minus the number of free parameters, i.e.:

$$\text{Residuals} = \frac{\Sigma_i^N (f(x_i) - y_i)^2}{N - N_p} \quad (18)$$

where N is the number of data points and N_p is the number of free parameters.

Comparison of the rate of formation of new nuclei via primary nucleation of α-syn under quiescent conditions in the presence and absence of SUVs. *Quiescent conditions in the absence of SUVs.* To compare the rate of formation of new nuclei via primary nucleation of α-syn under quiescent conditions in the presence and absence of SUVs, we first estimated the upper bound of this rate in the absence of SUVs. We have recently shown that under quiescent conditions and in the absence of SUVs the rate of secondary nucleation is negligible at pH values above 6 (ref. 36). Our data shows that in the absence of SUVs, no fibrils are detected when 140 μM α-syn is incubated under quiescent conditions during 125 h (**Supplementary Fig. 6**), suggesting that the rate of primary nucleation under such conditions is much lower than in the presence of SUVs. Despite the lack of observed aggregation, we can define an upper bound for the rate of primary nucleation in the absence of SUVs by assuming that under these conditions the mechanism of aggregation of α-syn consists of a nucleation step followed by elongation and that the total mass of fibrils varies with time according to ref. 46:

$$M(t) = m(0)[1 - (\text{sech}(\sqrt{\tfrac{n}{2}}\lambda t))^{2/n}] \quad (19)$$

with $\lambda = \sqrt{2k_n k_+ m(0)^n}$. The lowest ThT signal that we measured corresponds to the formation of 4 μM fibrils and is 10× higher than the signal of the background (**Supplementary Fig. 6**). We can thus assume that the minimum concentration of fibrils that we can detect using our experimental setup is approximately 0.4 μM, therefore putting an upper bound on the concentration of fibrils formed after 125 h. We thus estimated the upper limit of the rate of formation of new nuclei via primary nucleation ($k_n m(0)^n$) of α-syn under quiescent conditions using equation (19) and the following values for the different constants: M(t) ~0.4 μM, $k_+ = 2 \times 10^3\ s^{-1}$, $n = 2$ and m(0) = 140 μM and obtained a value of 7×10^{-18} M s^{-1}. It is worth mentioning that any contribution from secondary processes, which have been assumed to be negligible in the above equation, would render this value even smaller.

Quiescent conditions in the presence of SUVs. The global analysis of our data sets have shown that in the presence of SUVs, $k_n k_+ = 1.2 \times 10^{-5}\ M^{-(n+1)}\ s^{-2}$. For initial concentrations of α-syn free and α-syn bound to the SUVs of 140 μM and 10 μM, respectively, we can estimate the rate of formation of new nuclei via primary nucleation ($k_n b m(0)^n$) to be 1×10^{-14} M s^{-1}. Under these conditions, the presence of SUVs thus enhanced the rate of formation of new nuclei via primary nucleation of α-syn by a factor of 10^3.

Atomic force microscopy. *Data acquisition.* For atomic force microscopy (AFM) imaging, samples were diluted to ~1 μM total protein concentration into dH_2O, and 10 μl were pipetted onto freshly cleaved mica (Agar Scientific, Stansted, UK) and left to dry.

The samples were imaged with a Nanowizard II atomic force microscope (JPK Instruments, Waterbeach, UK) in intermittent contact mode in air, using NSC 36 cantilevers (Mikromasch, Tallinn, Estonia) with resonant frequencies between 70 kHz and 150 kHz.

Length distribution analysis. To evaluate the number of nucleation sites per vesicle, we estimated the number of fibrils and SUVs in solution by analyzing AFM images of the sample taken at the end of the reaction of amyloid formation, when 200 μM α-syn were incubated in the presence of 600 μM DMPS and led to the conversion of 40 μM α-syn into fibrils (**Fig. 5a**). First, we estimated the concentration of vesicles in solution formed by 600 μM DMPS. We showed that there are 6,000 DMPS lipids per SUVs; we thus estimated the concentration of SUVs in solution to 0.1 μM ($[\text{SUVs}] = \frac{\text{concentration of molecules of DMPS}}{\text{number of molecules of DMPS per SUV}}$). Second, the concentration of fibrils in solution was calculated as follows. We estimated the average length of α-syn fibrils by measuring the length distribution of the fibrils on the AFM image (**Fig. 5a**). The average length of the fibril formed was estimated to be 375 nm, which corresponds to ~400 monomers per fibril

$$\frac{\text{length}(\frac{\text{width}}{2})^2 \pi \rho N_A}{M},$$

where width = 5 nm, ρ = 1.35 g cm^{-3} (ref. 57), N_A is Avogadro's number and M is the molecular mass of α-syn. The concentration of fibrils can then be estimated to 0.1 μM ($[\text{fibrils}] = \frac{[\alpha - \text{syn}_{\text{fibrils}}]}{\text{number of monomer per fibril}}$, $[\alpha\text{-syn}_{\text{fibrils}}] = 40\ \mu M$), which corresponds to the concentration of SUVs in solution, suggesting that there is of the order of one nucleation event per SUV on average.

51. Hoyer, W. *et al.* Dependence of α-synuclein aggregate morphology on solution conditions. *J. Mol. Biol.* **322**, 383–393 (2002).
52. Petrache, H.I. *et al.* Structure and fluctuations of charged phosphatidylserine bilayers in the absence of salt. *Biophys. J.* **86**, 1574–1586 (2004).
53. Baldwin, A.J. *et al.* Metastability of native proteins and the phenomenon of amyloid formation. *J. Am. Chem. Soc.* **133**, 14160–14163 (2011).
54. Weinreb, P.H., Zhen, W., Poon, A.W., Conway, K.A. & Lansbury, P.T. Jr. NACP, a protein implicated in Alzheimer's disease and learning, is natively unfolded. *Biochemistry* **35**, 13709–13715 (1996).
55. Buell, A.K. *et al.* Frequency factors in a landscape model of filamentous protein aggregation. *Phys. Rev. Lett.* **104**, 228101 (2010).
56. Wales, D.J. & Doye, J.P.K. Global optimization by basin-hopping and the lowest energy structures of Lennard-Jones clusters containing up to 110 atoms. *J. Phys. Chem. A* **101**, 5111–5116 (1997).
57. Smith, J.F., Knowles, T.P., Dobson, C.M., Macphee, C.E. & Welland, M.E. Characterization of the nanoscale properties of individual amyloid fibrils. *Proc. Natl. Acad. Sci. USA* **103**, 15806–15811 (2006).